Large-Signal Response of Semiconductor Quantum-Dot Lasers

Kathy Lüdge, Roland Aust, Gerrit Fiol, Mirko Stubenrauch, Dejan Arsenijević, Dieter Bimberg, *Fellow, IEEE*, and Eckehard Schöll

Abstract—In this paper, the large-signal response of a quantum-dot laser is investigated. Based on experimental results, we show that including a dynamic device temperature as well as Auger recombination processes in the carrier reservoir is crucial to model the dynamic response of a quantum-dot laser for large variations of the pump current. A detailed analysis of the influence of temperature effects on the dynamics of the device is performed. Simulated eye diagrams are presented and compared with experimental results at the emission wavelength of 1.3 μ m.

Index Terms—Dynamic temperature, eye diagrams, largesignal response, quantum-dot laser.

I. INTRODUCTION

PUTURE high-speed data communication applications demand devices that are insensitive to temperature variations and optical feedback effects and provide features like high modulation bandwidth, low chirp, as well as error-free operation. Currently, self-organized semiconductor quantum-dot (QD) lasers already provide many of those requirements [1]–[3]. Previous works on nonlinear dynamics of QD lasers [4]–[6] have examined the turn-on behavior and small-signal response of such devices validated by experimental measurements.

In this paper, we focus on the large-signal response of semiconductor QD lasers. The modeling approach is based on a rate equation model incorporating microscopically calculated carrier–carrier scattering rates. It enables a quantitative modeling of the QD laser output without assuming fit parameters for the carrier lifetimes and can be considered as a model on an intermediate level between a fully microscopic quantum kinetic treatment including polarization and population dynamics [7]–[10] and a system of phenomenological rate equations with constant coefficients [11].

Based on experimental lasing spectra that show an increase in the lasing linewidth with increasing pump current, we

Manuscript received June 8, 2010; revised July 23, 2010; accepted July 31, 2010. Date of current version November 24, 2010. This work was supported in part by the Deutsche Forschungsgesellschaft in the framework of Sfb787.

K. Lüdge, R. Aust, and E. Schöll are with the Institut für Theoretische Physik, Technische Universität Berlin, Berlin 10623, Germany (e-mail: luedge@physik.tu-berlin.de; roland.aust@tu-berlin.de; schoell@physik.tu-berlin.de).

G. Fiol, M. Stubenrauch, D. Arsenijević, and D. Bimberg are with the Institut für Festkörperphysik, Technische Universität Berlin, Berlin 10623, Germany (e-mail: gerrit.fiol@physik.tu-berlin.de; stubenrauch@sol.physik.tu-berlin.de; bimberg@physik.tu-berlin.de).

Color versions of one or more of the figures in this paper are available online at http://ieeexplore.ieee.org.

Digital Object Identifier 10.1109/JQE.2010.2066959

extend our previous model [12] by taking into account the pump-current-dependent spectral properties of the active QDs. Furthermore, experimental findings on the device temperature during operation [13] are used to incorporate a dynamic temperature in the rate equations that increases with the pump current. We also improve the model with respect to the loss term in the equations for the carrier reservoir. In previous works, pure bimolecular recombination was used in order to model the carrier losses. The model presented here now separates the radiative losses (spontaneous emission) that can be calculated according to [14] and the Auger-related losses.

This paper is organized as follows. After introducing the experimental details and the theoretical model in Sections II and III, respectively, we discuss the dependence of the large-signal response upon the dynamic parameters in Section IV. In Section V, we compare experimental and theoretical eye pattern diagrams of the QD laser, and we conclude in Section VI.

II. EXPERIMENTAL RESULTS

The laser investigated here is a ridge waveguide InAs/InGaAs QD laser diode. The diode incorporates 15 stacks of QD layers having a dot-in-a-well (DWELL) structure [15]. The ridge is etched through the active layer to reduce current spread [16] and to enhance wave guiding. The width of the ridge is $4 \mu m$, while the length is 1 mm. To use the diode in high-frequency modulation schemes, top p- and ncontacts in a ground-signal-ground configuration, allowing the use of high-speed low-loss probe heads, have been processed. The threshold current density j_{th}^{exp} at room temperature is $380\,\mathrm{A\,cm^{-2}}$ with an emission wavelength close to $1.3\,\mu\mathrm{m}$ (see Fig. 1). For all pump currents, no excited-state lasing is found. Both facets of the laser are as cleaved. The diode is mounted on a copper heat sink and the light output is coupled to a standard single-mode fiber. A fiber-based isolator is used to prevent any feedback from influencing the laser diode. Eye diagrams have been obtained with an Agilent ParBert system, which creates an electrical pseudo-random binary sequence (PRBS) in a non-return-to-zero configuration. Here a PRBS 5 (length: $2^5 - 1$ bit) is used to make the results comparable to theoretical calculations. The sequence of bits (here 31) is called a word.

Fig. 2 shows the optical response of the laser to an electrical PRBS 5 signal switching between two levels $(1.5 j_{th})$ and $(3 j_{th})$ of continuous wave (CW) operation. Simulated and

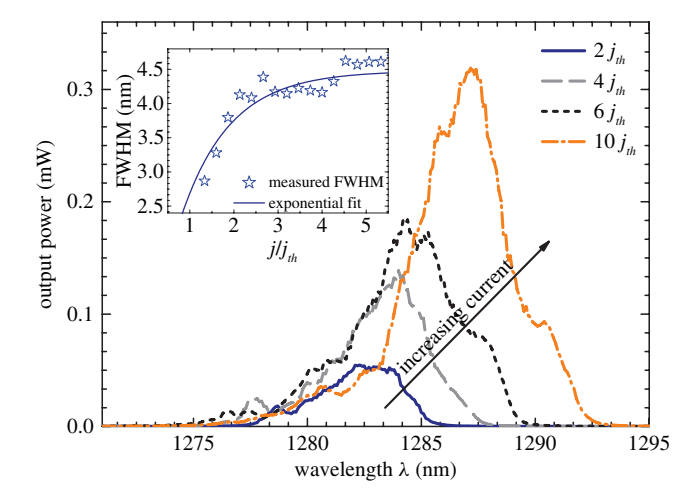


Fig. 1. Experimental lasing spectra for increasing pump currents illustrating the increasing number of longitudinal modes. Inset: Exponential fit of full-width-at-half-maximum (FWHM) = $4.48-4.41 \exp(-0.06 \cdot j/j_{th})$ (blue solid line) and FWHM of the measured spectra (blue stars).

experimentally determined input signals (electrical words) are shown in the upper panel of Fig. 2. Due to the experimental setup (e.g., influence of cables and divider, oscilloscope noise), the measured pump-current signal (black line) is not as flat as the simulated time trace (red line). Despite this small deviation, the measured optical response (black line, lower panel) matches the simulated laser output (red line, lower panel) very well. By superposing this sequence bitwise, an eye diagram [17] is generated, which will be discussed in Section V. The details of the theoretical modeling will be discussed in the following sections.

The frequency and amplitude of the PRBS signal can be varied. In the subsequent analysis, we fix the modulation amplitude and vary the frequency between 2.5 and 10.0 GHz. The electrical modulation signal and the laser pump current are combined using a bias-T. Subsequently, they are transmitted to the laser diode using high-frequency cables and the high-speed low-loss probe heads. The modulation bandwidth of the laser is 7.0 GHz taken from transmission measurements using a fully calibrated network analyzer, proving the ability of the laser to generate 10.0 Gbit/s open eye diagrams [18]. The modulated optical signal is detected by a photoreceiver together with a high-speed sampling oscilloscope. All equipment used has a sufficiently high bandwidth in order not to distort the eye diagrams recorded. The setup for measuring relaxation oscillations (ROs) can be found in [6].

III. Model

The model used for the simulations is based on the microscopic model used in [12] and [19]. It describes a QD laser system, where the carriers are first injected into the carrier reservoir of the device before they are captured by the QDs. The carrier reservoir of the DWELL structure is modeled by a 4-nm-wide layer, as in our previous work [12], [19], but here the more appropriate acronym quantum well (QW) is used rather than wetting layer (WL), in order to avoid confusion with the more common notion of a monomolecular WL.

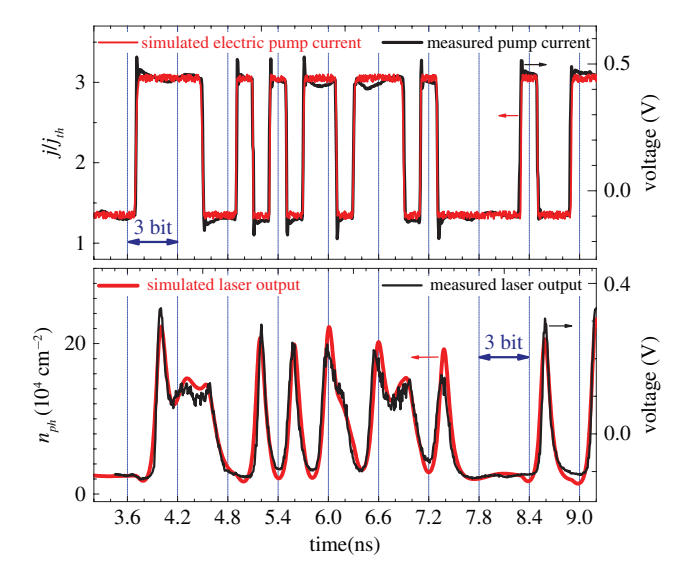


Fig. 2. Comparison between simulated (red line) and measured data (black line) of the electrical input signal (upper panel) and optical output (lower panel) vs. time. Vertical lines show the separation into 3-bit sequences.

A sketch of the epitaxial structure as well as the energy diagram of the band structure is shown in Fig. 3(a) and (b), respectively. We consider a two-level system for electrons and holes in the QDs. The carrier relaxation processes within the QD states are much faster (approximately picoseconds) than the capture processes from the QW into the QDs at high QW carrier densities [20], so that all higher QD levels can be adiabatically eliminated. As a result, only the energetically lowest electron and hole levels in the QDs contribute crucially to the laser dynamics [21]. The fast phonon-assisted carrier relaxation processes within the QW states are taken into account by assuming a quasi-Fermi distribution with quasi-Fermi levels F_e^{QW} and F_h^{QW} inside the conduction and the valence band of the QW, respectively.

$$\dot{n}_e = S_e^{in} (N^{QD} - n_e) - S_e^{out} n_e - R_{ind} - R_{sp} \tag{1}$$

$$\dot{n}_h = S_h^{in} (N^{QD} - n_h) - S_h^{out} n_h - R_{ind} - R_{sp}$$
 (2)

$$\dot{w}_{e} = \eta \frac{\dot{j}(t)}{e_{0}} - \frac{N^{sum}}{NQD} \left[S_{e}^{in} (N^{QD} - n_{e}) - S_{e}^{out} n_{e} \right] - R_{loss}$$
(3)

$$\dot{w}_{h} = \eta \frac{\dot{j}(t)}{e_{0}} - \frac{N^{sum}}{N^{QD}} \left[S_{h}^{in} (N^{QD} - n_{h}) - S_{h}^{out} n_{h} \right] - R_{loss}$$
(4)

$$\dot{n}_{ph} = -2\kappa n_{ph} + \Gamma R_{ind} + \beta R_{sp} \tag{5}$$

The nonlinear rate equations (1)–(5) describe the dynamics of the charge carrier densities in the QDs (n_e and n_h), the carrier densities in the QW (w_e and w_h) (e and h stands for electrons and holes, respectively), and the photon density n_{ph} . The induced processes of absorption and emission are modeled by a linear gain $R_{ind} = WA(n_e + n_h - N^{QD}) n_{ph}$, where N^{QD} denotes twice the QD density of the lasing subgroup (the factor of two accounts for spin degeneracy). As a result of the size distribution and material composition fluctuations of the QDs, only a subgroup (density N^{QD}) of all QDs (N^{sum}) matches the mode energies for lasing. As will be discussed below,

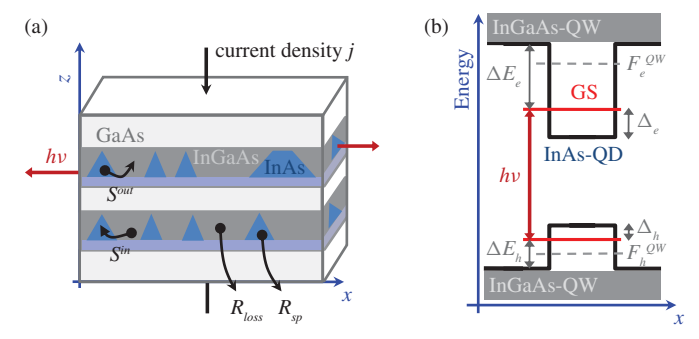


Fig. 3. (a) Schematic illustration of the DWELL structure of the QD laser. (b) Energy diagram of the band structure across a QD. $h\nu$ labels the ground-state (GS) lasing energy. ΔE_e and ΔE_e mark the distance of the GS from the QW band edge for electrons and holes, respectively. Δ_e and Δ_h denote the distance to the bottom of the QD. F_e^{QW} and F_h^{QW} are the quasi-Fermi levels for electrons and holes in the QW, respectively.

 N^{QD} is not a constant but increases with increasing pump current due to the increasing number of longitudinal modes in the laser output (see Fig. 1). The Einstein coefficient W is given by $W = [(|\mu|^2 \sqrt{\epsilon_{bg}})/(3\pi \epsilon_0 \hbar)](\omega/c)^3$, where ϵ_{bg} is the static relative permittivity of the background medium, ε_0 is the vacuum permittivity, c is the speed of light in vacuum, and μ is the dipole moment of the QDs. A is the in-plane area of the QW. Analogous to a simple two-level system, our model yields positive gain if the occupation probability $f_e^C = n_e/N^{QD}$ of electrons in the localized conduction band level of the QDs is higher than the occupation probability f_e^V of electrons in their localized valence band level. In the hole picture, the occupation probability of holes in the localized valence band level is given by $f_h^V = 1 - f_e^V = n_h/N^{QD}$. Thus our gain term $R_{ind} = WAN^{QD}(f_e^C - f_e^V)n_{ph} = WAN^{QD}\left(f_e^C(1 - f_e^V) - f_e^V(1 - f_e^C)\right)n_{ph}$ corresponds to the standard net rate of stimulated emission minus absorption [14].

The spontaneous emission in the QDs is approximated by $R_{sp}(n_e, n_h) = (W/N^{QD})n_e n_h$. The rate $R_{loss} = B(w_e)w_e w_h$ accounting for carrier losses in the QW is a sum of the spontaneous band-band recombination $B^S w_e w_h$ and Augerrelated losses given by $B_A w_e w_e w_h$ describing Auger scattering processes inside the QW. The density N^{sum} is twice the total QD density as given by experimental surface imaging (again, the factor two accounts for spin degeneracy). β is the spontaneous emission coefficient and $\Gamma = \Gamma_g N^{QD}/N^{sum}$ is the optical confinement factor. Γ is the product of the geometric confinement factor Γ_{ϱ} (i.e., the ratio of the volume of all QDs and the mode volume) and the ratio N^{QD}/N^{sum} (accounting for reduced gain since only a subgroup of all QDs matches the mode energy for lasing due to the size distribution and material composition fluctuations of the QDs). The coefficient $2\kappa = (c/\sqrt{\varepsilon_{bg}})[\kappa_{int} - \ln(R_1R_2)/2L]$ expresses the total cavity loss [22], where L is the cavity length, and R_1 , R_2 are the facet reflectivities and κ_{int} are the internal losses [6]. j is the injection current density, e_o is the elementary charge, and $\eta = 1 - w_e/N^{QW}$ is the current injection efficiency that accounts for the fact that we cannot inject any more carriers if the QW is already filled (maximum density inside the QW: $w_e = N^{QW}$). Note that in our model the carriers are directly

TABLE I
NUMERICAL PARAMETERS USED IN THE SIMULATION
UNLESS STATED OTHERWISE

Symbol	Value	Symbol	Value
W	0.7 ns ⁻¹	A	$4 \times 10^{-5} \text{ cm}^2$
T	Eq. (6)	N^{QD}	Eq. (8)
B	Eq. (7)	N^{sum}	$20 \times 10^{10} \text{ cm}^{-2}$
Γ_g	0.075	N^{QW}	$1 \times 10^{12} \text{ cm}^{-2}$
2κ	0.1 ps^{-1}	β	5×10^{-6}
μ	$0.75 e_0 \text{ nm}$	m_h	$0.45 m_0$
ε_{bg}	14.2	m_e	$0.043 \ m_0$
ΔE_e	210 meV	ΔE_h	50 meV
Δ_e	64 meV	Δ_h	6 meV
$ ho_e$	$m_e/(\pi \hbar^2)$	$ ho_h$	$m_h/(\pi \hbar^2)$
κ_{int}	220 m^{-1}	L	1 mm
R_1, R_2	0.32	\dot{J}_{th}	65 A cm ⁻²

injected into the QW, leading, of course, to an underestimation of the experimentally realized current densities. Therefore, only current densities relative to the threshold value j_{th} are considered for comparisons between theory and experiment.

The spectral properties of the laser output are not addressed in the model, as the photon density is an average over all longitudinal modes inside the cavity. Changes in the number of longitudinal modes are taken into account by changes in the active QD density N^{QD} , which basically changes the gain of the active medium. With a given QD size distribution ρ_i (where i is the index for a certain longitudinal mode frequency v_i), the QD density participating in the emission at a given frequency v_i is $N_i^{QD} = \rho_i N^{sum}$. Thus, the density of all active QDs is given by $N^{QD} = \sum_k \rho_k N^{sum}$ (the index k denotes the lasing longitudinal modes). The mode spacing inside the cavity (L = 1 mm) is $\Delta h \nu = 0.17 \text{ meV}$ ($\Delta \lambda = 0.22 \text{ nm}$), while the standard deviation of the QD size distribution [22] is about $\sigma_{inh} = 65 \text{ meV} = 380 \Delta h v$. Thus, 70% of all QDs (0.7 N^{sum}) are active if the laser emits light at 380 longitudinal modes. Lasing spectra taken from the OD laser at different pump currents (Fig. 1) show an FWHM between 2.7 nm \equiv 12 modes and $4.5 \,\mathrm{nm} \equiv 20 \,\mathrm{modes}$. The functional dependence of the FWHM upon the pump current has been fitted as shown in the inset of Fig. 1. Using this relation, we can estimate the value of N^{QD} by using $N^{QD}/N^{sum} = (FWHM/\Delta\lambda)/(380/0.7)$, which will be used later on for improving the model. The values of parameters used in our simulations are listed in Table I, if not stated otherwise.

Another important contribution to the dynamics of QD lasers are the non-radiative carrier–carrier scattering processes between the QD and the QW. The scattering rates S_e^{in} , S_e^{out} , S_h^{in} , and S_h^{out} of electrons (e) and holes (h) for scattering in and out of the QDs are a measure of the strength of these processes. We derive these rates microscopically as a nonlinear function of the QW carrier densities w_e and w_h as described in detail in [4] and [12]. The Auger scattering rates depend on the carrier temperature inside the QW. In our previous works [3]–[6], [12], [19], T was held constant at room temperature 300 K. Here we perform microscopic calculations for several temperatures (the results for T=350 and 400 K are plotted in Fig. 4) and subsequently fit the results with the following analytic expression in order to allow for an

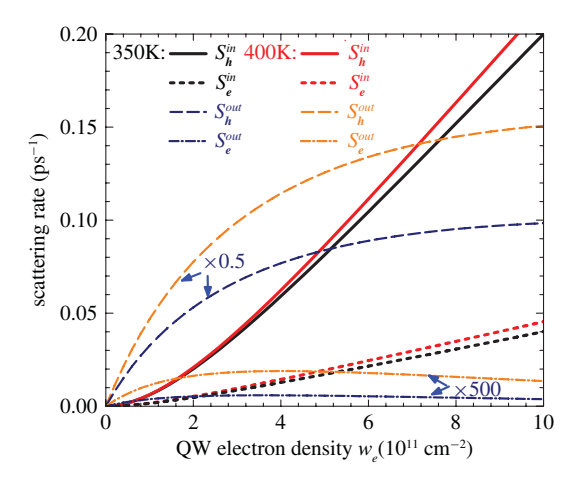


Fig. 4. Scattering rates between QW and QD as a function of w_e and $w_h = 2w_e$ for electron scattering into (dotted lines) and out of (dash-dotted lines which are multiplied by 500) the QD, as well as hole in-scattering (solid lines) and out-scattering (dashed lines multiplied by 0.5) for two different temperatures T = 350 K (black/blue) and T = 400 K (red/orange).

implementation into the rate equations:

$$S_e^{in}(T, w_e, w_h) = \frac{9T + 300 K}{3000 K} \cdot S_e^{in}(300 K, w_e, w_h)$$

$$S_h^{in}(T, w_e, w_h) = \frac{0.75T + 300 K}{525 K} \cdot S_h^{in}(300 K, w_e, w_h).$$

The out-scattering rates are related to the in-scattering rates by detailed balance as derived in [12] and [19]:

$$S_{e}^{out}(T, w_{e}, w_{h}) = S_{e}^{in}(T, w_{e}, w_{h}) \cdot \frac{e^{-\frac{\Delta E_{e}}{kT}}}{e^{\frac{w_{e}}{\rho_{e}kT}} - 1}$$
$$S_{h}^{out}(T, w_{e}, w_{h}) = S_{h}^{in}(T, w_{e}, w_{h}) \cdot \frac{e^{-\frac{\Delta E_{h}}{kT}}}{e^{\frac{w_{h}}{\rho_{h}kT}} - 1}.$$

Here, ΔE_e and ΔE_h are the energy separations between the QD electron and hole GS and the lowest respective QW state [see Fig. 3(b)]. $\rho_e = m_e/(\pi\hbar^2)$ and $\rho_h = m_h/(\pi\hbar^2)$ are the respective 2-D densities of state in the QW.

IV. DYNAMIC PARAMETERS

In this section, we extend our previous model by incorporating self-consistently three dynamic effects that occur with increasing injection current density. For the shift of the device temperature inside an electrically pumped optical amplifier (with identical active region as the laser-diode considered here), Gomis-Bresco *et al.* [13] found values of $\Delta T = 60 \text{ K}$ at a pump current of I = 150 mA, which is about 10 times the threshold current of the laser investigated here. Their measurement suggests a functional relationship of $\Delta T(j) \sim j^2$. Since this temperature change is due to an increasing QW carrier density, and the QW carrier density itself depends via $w_e \sim \sqrt{j}$ (see [12]) on the pump current, we implement $\Delta T(w_e) \sim (w_e)^4$ as given by (6)

$$T = 300 K + 0.245 \cdot 10^{12} \text{nm}^8 (w_e)^4.$$
 (6)

The term describing the losses inside the QW ($R_{loss} = Bw_ew_h$), which in our previous works [19] was implemented solely as bimolecular recombination with constant B, has been

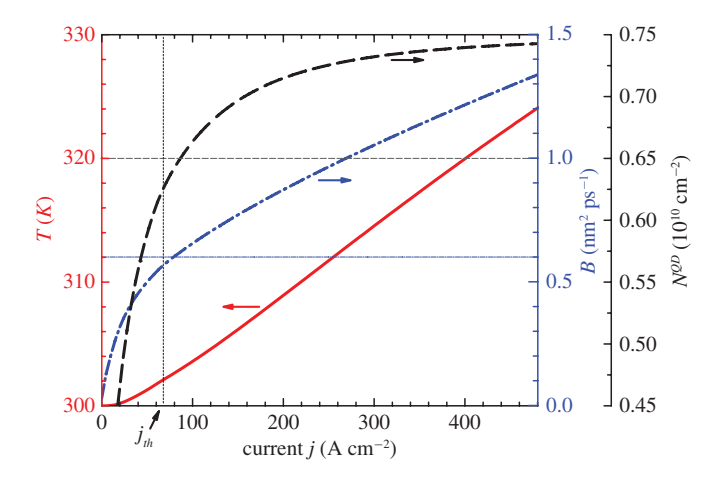


Fig. 5. Temperature T (solid red), carrier reservoir loss coefficient B (dash-dotted blue), and active QD density N^{QD} (dashed black) according to (6)–(8), respectively, at CW operation as a function of the pump current density j.

extended in order to distinguish between Auger recombination inside the QW and bimolecular recombination processes. The Auger rate varies with the third order in the QW carrier density. We approximate *B* by

$$B = B^{S} + B_{A}w_{e}$$

$$= 0.03 \text{ nm}^{2}\text{ps}^{-1} + 305 \text{ nm}^{4}\text{ps}^{-1} \left(\frac{T}{300 \text{ K}}\right)^{4} w_{e}.$$
 (7)

The Auger coefficient B_A has been shown to depend significantly on the temperature T [23] and is therefore implemented in (6) such that it leads to a doubling of the rate for a temperature change of 60 K. The value for B^S is determined by integrating in **k**-space over all possible transitions between the occupied electron states in the conduction band (occupation probability f_k^e at energy E_k^e) and occupied hole states in the valence band (occupation probability f_k^h at energy E_k^h). This gives $\widetilde{R}_{sp} = 1/A \sum_{k=0}^{\infty} W_k f_k^e \cdot f_k^h$, where $W_k = \left((|\mu|^2 \sqrt{\varepsilon_{bg}})/(3\pi \hbar^4 c^3 \varepsilon_0) \right) (E_k^e - E_k^h)^3$ is the optical transition rate for the QW. The full integral cannot be solved analytically. However, for the case of non-degenerate carrier concentrations, analytic approximations are possible [14], leading to $\widetilde{R}_{sp} \approx W_{k=0} \left((m_r \pi \hbar^2)/(m_e m_h kT) \right) w_e w_h = 0.03 \text{ nm}^2 \text{ ps}^{-1} w_e w_h$, where m_r denotes the reduced mass.

In extension of the model used in [12] and [19], also N^{QD} is implemented as a function of the QW carrier density. This is motivated by the experimental lasing spectra shown in Fig. 1, which shows increasing width and thus indicate an increasing number of longitudinal modes in the spectra with increasing pump current. According to the experimental data (inset of Fig. 1), we implement the functional dependence as follows:

$$\frac{N^{QD}}{10^{-4}\text{nm}^{-2}} = 0.75 - 0.74 \exp\left(-\frac{10^6}{1.75}w_e^2\right).$$
 (8)

To visualize the dependence of these three dynamic parameters on the pump current under CW operation, we plot their values in Fig. 5.

The effect of implementing $T(w_e)$, $B(w_e)$, and $N^{QD}(w_e)$, according to (6)–(8), on the photon output is shown in Fig. 6. It depicts the photon density of the QD laser if subjected to

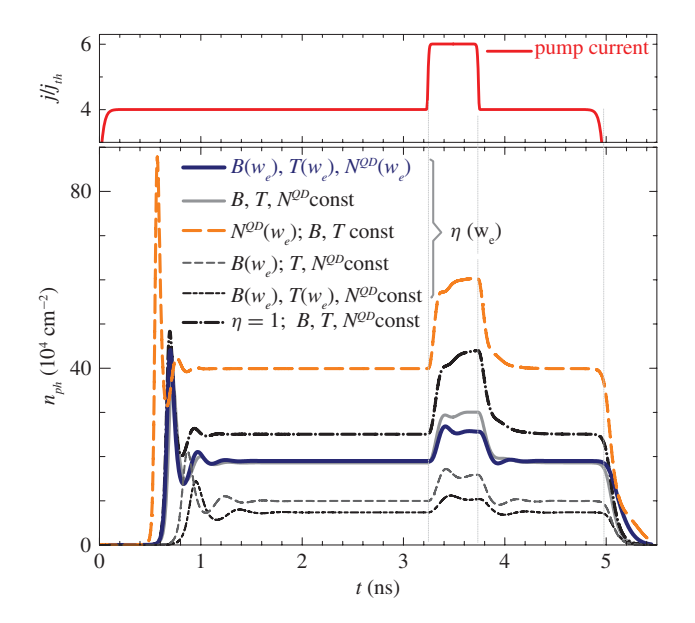


Fig. 6. Transient dynamics of the photon density (lower panel) resulting from a pump pulse (red solid line in the upper panel) of $j=4\,j_{th}$ between 0 and 5 ns and $j=6\,j_{th}$ between 3.3 and 3.8 ns. Different lines correspond to different combinations of constant and density-dependent values for T,B, and N^{QD} [see (6)–(8)] as indicated in the legend.

an electric current pulse that at first switches the laser on at t = 0 with $j = 4 j_{th}$, then switches to $j = 6 j_{th}$ for 3.3 ns $\leq t \leq 3.8$ ns, and finally turns it off at t = 5 ns. The thick blue line corresponds to the full model with dynamic parameters and injection efficiency $\eta = 1 - w_e/N^{QW}$, while the dashdotted black line refers to constant values of T, N^{QD} , B, and $\eta = 1$ as used in [12]. While the turn-on dynamics shows that the strongly damped ROs are basically unaffected if all three parameters become j-dependent, the large-signal response of the laser changes dramatically. For the case of constant values, the photon density very slowly reaches the new steady state upon switching, which is related to the slow increase of the QW carrier density (time scale $\tau_e^{QW} = (Bw_h)^{-1} \approx 0.4$ ns at $j = 4 j_{th}$). With dynamic parameters, on the other hand, the large-signal response shows a small relaxation peak during upand down-switching (thick blue line between t = 3 and 4 ns in Fig. 6).

This small relaxation peak is nearly what is experimentally found for the QD laser as can be seen in Fig. 2, which shows the laser response to a bit sequence. The faster increase of n_{ph} at j=4 j_{th} can be explained by the shorter time scale of the QW carrier losses being reduced to $\tau_e^{QW} \approx 0.3$ ns. Using $\eta(w_e)$ and keeping constant values for T, B, and N^{QD} already improve the laser response during switching at high currents but does not yield the correct relaxation peak (thick gray line). Fig. 6 also shows the discussed laser response if besides $\eta(w_e)$ only $N^{QD}(w_e)$ increases with the current (dashed orange line showing very slow increase of n_{ph}), if only $B(w_e)$ increases with current (short-dashed dark gray line showing a pronounced relaxation peak but slow RO frequency) or $B(w_e)$ and $T(w_e)$ increase with current (dash-dot-dotted black line showing further reduction in gain and RO frequency).

Fig. 7(a) and (b) summarizes the RO frequency and the turnon delay time of the QD laser for the different parameter sets

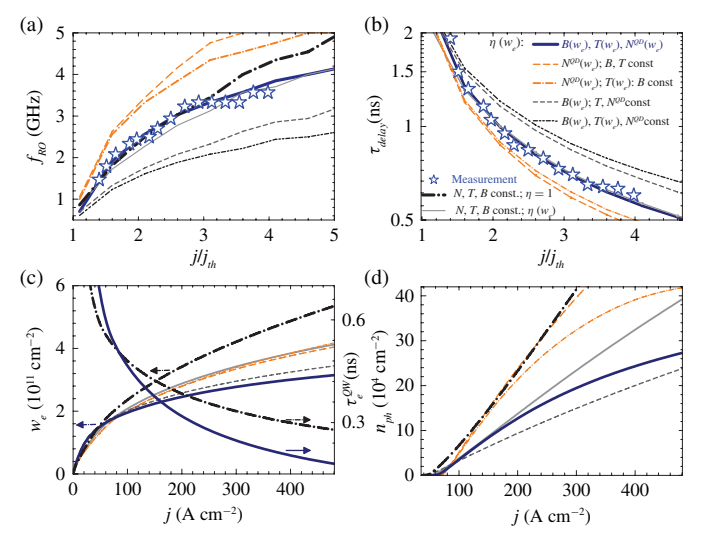


Fig. 7. Laser turn-on behavior: (a) RO frequency and (b) turn-on delay time as a function of the normalized pump current j/j_{th} . (c) and (d) show the steady-state QW electron density [left axis in (c)], steady-state QW electron lifetime $\tau_e^{QW} = (Bw_h)^{-1}$ [right axis in (c)], and steady-state photon density (d) as a function of pump current j. Different lines correspond to different combinations of constant and density-dependent values for T, B, and N^{QD} as indicated in the legend. Stars are the measured data.

discussed in Fig. 6 for pump currents up to $5j_{th}$, and compare them to experimental data. It can be seen that the deviation of the simulated curve with constant parameters (dash-dotted black line) from the measured RO frequency [stars in Fig. 7(a)] at currents larger than 3 j_{th} vanishes if the full dynamic model is chosen (thick blue line). Smaller injection efficiency (gray line), dynamic and thus higher B (dashed gray line), and dynamic and thus higher T (dash dot dotted black line) reduce the RO frequency and at the same time increase the delay time τ_{delay} . Solely increasing N^{QD} (dashed orange line) leads to very high RO frequencies that do not match the experimental data. Fig. 7(c) and (d) depicts the steady-state QW electron density, the time scale of the carrier losses inside the QW τ_e^{QW} , and the photon density at steady state as a function of the pump current j for all parameter sets discussed earlier in Fig. 7(a) and (b). Together with Fig. 6, this shows that the large-signal response of the laser is influenced only by variations in the QW carrier density and the related lifetime τ_e^{QW} , while changes in the gain as invoked by T and N^{QD} just affect the intensity of the laser output but not the qualitative shape of the transients $n_{ph}(t)$ during switching. Introducing a QW temperature that increases with the current leads to a strong reduction in the differential gain as can be seen in the laser characteristics shown in Fig. 7(d) (dotted orange and thick blue curve).

V. EYE DIAGRAMS

From the discussion in the last section, we conclude that it is necessary to incorporate the dynamic increase of B and N^{QD} with w_e as described by (7) and (8) in order to simulate eye diagrams of large-signal response observed in the experiment. Using $B(w_e)$ alone leads to RO frequencies that are much too low when compared to the experimental results. Note again that the increase of N^{QD} with current is motivated by the measured lasing spectra shown in Fig. 1. To meet the RO

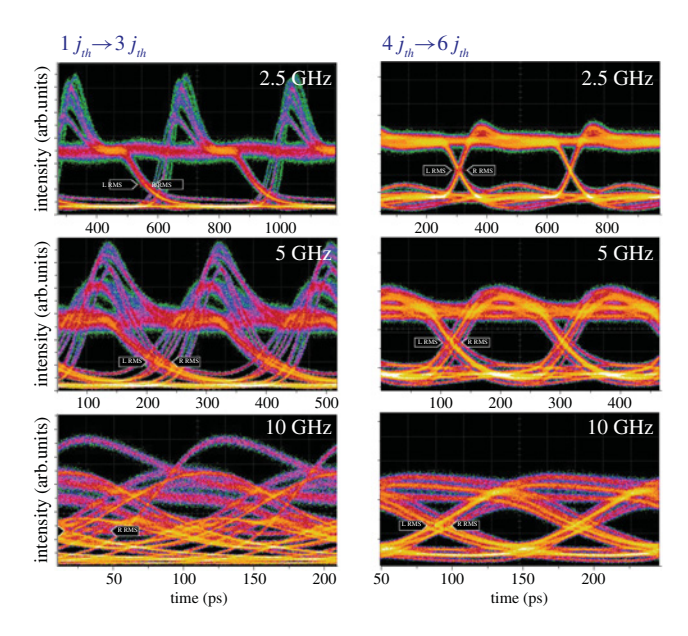


Fig. 8. Measured eye diagrams for pump currents switching between 1 j_{th} and 3 j_{th} (left column) and between 4 j_{th} and 6 j_{th} (right column). Bit repetition frequency varies between 2.5 (first line) and 10.0 GHz (third line).

frequencies observed in experiment at higher pump currents, an increasing temperature $T(w_e)$ as given by (6) has to be implemented.

Using the dynamic dependencies listed above, it is possible to accurately model the measured eye diagrams. This can be seen in Figs. 8 and 9, which show the measured and simulated eye patterns, respectively, for switching between two different current levels (left column: $j_{th} \mapsto 3 j_{th}$ and right column: $4 j_{th} \mapsto 6 j_{th}$) and for three different pulse repetition frequencies (2.5, 5.0, and 10.0 GHz). We find exact agreement in the shape (overshoots, trace, and extinction ratio) of the calculated and measured diagrams. By comparing the laser response for the different current levels, we can conclude that, in order to improve the eye pattern diagrams, it is better to use higher current levels as thereby the relaxation peaks are suppressed. The cutoff frequency of this QD laser—which is related to its RO frequency of 7.0 GHz—leads to a closing of the eyes already at 10.0 GHz. This can be improved by using higher pump currents, however, our modeling predicts that there is a tradeoff since at the same time device heating results in further reduction of the RO frequency.

VI. CONCLUSION

In conclusion, we have extended our microscopic rate equation model by including heating effects, pump-dependent spectral properties, and Auger recombination losses in the carrier reservoir. This has not been done by merely including a static dependence upon the pump current j, but rather by a fully self-consistent dynamic dependence of the temperature, the number of longitudinal modes, and the loss rate upon the QW carrier density w_e which is calculated dynamically from the coupled rate equations in dependence upon j. Thus we could not only describe correctly the current dependence under CW operation, but also predict the transient large-signal response over a large range of pump currents. We have found that an increasing temperature leads to a reduction of the RO

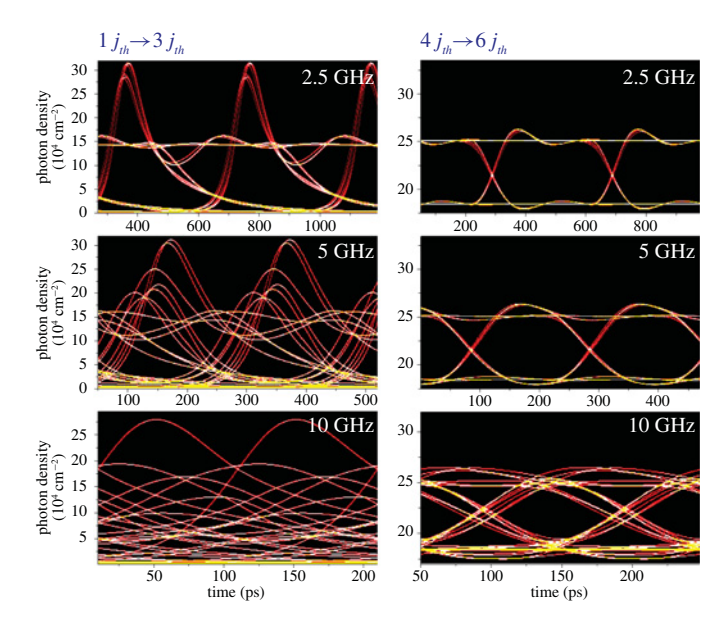


Fig. 9. Simulated eye diagrams for dynamic parameters for T, B, and N^{QD} according to (6)–(8) for pump currents switching between 1 j_{th} and 3 j_{th} (left column) and between 4 j_{th} and 6 j_{th} (right column) for three different bit repetition frequencies: 2.5 (first line), 5.0 (second line), and 10.0 GHz (third line).

frequency and thus to a reduction of the modulation bandwidth at higher pump currents. By comparing the experimental and simulated eye diagrams, we have found that decreasing injection efficiency into the QW and increasing carrier losses inside the QW at high QW carrier densities are crucial in order to correctly model the large-signal response of the QD laser.

REFERENCES

- [1] D. Bimberg, G. Fiol, M. Kuntz, C. Meuer, M. Lämmlin, N. N. Ledentsov, and A. R. Kovsh, "High speed nanophotonic devices based on quantum dots," *Phys. Stat. Sol.* (A), vol. 203, no. 14, pp. 3523–3532, Nov. 2006.
- [2] W. W. Chow and S. W. Koch, Semiconductor-Laser Fundamentals. Berlin, Germany: Springer-Verlag, 2004.
- [3] C. Otto, K. Lüdge, and E. Schöll, "Modeling quantum dot lasers with optical feedback: Sensitivity of bifurcation scenarios," *Phys. Stat. Sol.* (*B*), vol. 247, no. 4, pp. 829–845, Apr. 2010.
- [4] E. Malić, K. J. Ahn, M. J. P. Bormann, P. Hövel, E. Schöll, A. Knorr, M. Kuntz, and D. Bimberg, "Theory of relaxation oscillations in semiconductor quantum dot lasers," *Appl. Phys. Lett.*, vol. 89, no. 10, pp. 101107-1–101107-3, Sep. 2006.
- [5] E. Malić, M. J. P. Bormann, P. Hövel, M. Kuntz, D. Bimberg, A. Knorr, and E. Schöll, "Coulomb damped relaxation oscillations in semiconductor quantum dot lasers," *IEEE J. Sel. Topics Quantum Electron.*, vol. 13, no. 5, pp. 1242–1248, Sep.–Oct. 2007.
- [6] K. Lüdge, M. J. P. Bormann, E. Malić, P. Hövel, M. Kuntz, D. Bimberg, A. Knorr, and E. Schöll, "Turn-on dynamics and modulation response in semiconductor quantum dot lasers," *Phys. Rev. B*, vol. 78, no. 3, pp. 035316-1–035316-11, 2008.
- [7] M. Lorke, F. Jahnke, and W. W. Chow, "Excitation dependences of gain and carrier-induced refractive index," *Appl. Phys. Lett.*, vol. 90, no. 5, pp. 051112-1–051112-3, Jan. 2007.
- [8] H. C. Schneider, W. W. Chow, and S. W. Koch, "Excitation-induced dephasing in semiconductor quantum dots," *Phys. Rev. B*, vol. 70, no. 23, pp. 235308-1–235308-4, Dec. 2004.
- [9] W. W. Chow and S. W. Koch, "Theory of semiconductor quantum-dot laser dynamics," *IEEE J. Quantum Electron.*, vol. 41, no. 4, pp. 495–505, Apr. 2005.
- [10] J. Gomis-Bresco, S. Dommers, V. V. Temnov, U. Woggon, M. Lämmlin, D. Bimberg, E. Malić, M. Richter, E. Schöll, and A. Knorr, "Impact of Coulomb scattering on the ultrafast gain recovery in InGaAs quantum dots," *Phys. Rev. Lett.*, vol. 101, no. 25, pp. 256803-1–256803-4, Dec. 2008.

- [11] D. O'Brien, S. P. Hegarty, G. Huyet, and A. V. Uskov, "Sensitivity of quantum-dot semiconductor lasers to optical feedback," Opt. Lett., vol. 29, no. 10, pp. 1072-1074, May 2004.
- [12] K. Lüdge and E. Schöll, "Quantum-dot lasers-desynchronized nonlinear dynamics of electrons and holes," IEEE J. Quantum Electron., vol. 45, no. 11, pp. 1396–1403, Nov. 2009.
- [13] J. Gomis-Bresco, S. Dommers, V. V. Temnov, U. Woggon, J. Martinez-Pastor, M. Lämmlin, and D. Bimberg, "InGaAs quantum dots coupled to a reservoir of nonequilibrium free carriers," IEEE J. Quantum Electron., vol. 45, no. 9, pp. 1121-1128, Sep. 2009.
- [14] G. Lasher and F. Stern, "Spontaneous and stimulated recombination radiation in semiconductors," Phys. Rev., vol. 133, no. 2A, pp. A553-A563, 1964.
- [15] A. R. Kovsh, N. A. Maleev, A. E. Zhukov, S. S. Mikhrin, A. V. Vasil'ev, A. Semenova, Y. M. Shernyakov, M. V. Maximov, D. A. Livshits, V. M. Ustinov, N. N. Ledentsov, D. Bimberg, and Z. I. Alferov, "InAs/InGaAs/GaAs quantum dot lasers of 1.3 μm range with enhancedoptical gain," J. Crystal Growth, vol. 251, no. 1, pp. 729-736,
- [16] D. Ouyang, N. N. Ledentsov, D. Bimberg, A. R. Kovsh, A. E. Zhukov, S. S. Mikhrin, and V. M. Ustinov, "High performance narrow stripe quantum-dot lasers with etched waveguide," Semicond. Sci. Technol., vol. 18, no. 12, pp. L53-L54, 2003.
- [17] D. Derickson and M. Müller, Digital Communications Test and Measurement: High-Speed Physical Layer Characterization. Upper Saddle River, NJ: Prentice Hall, 2007.
- [18] M. Kuntz, G. Fiol, M. Lämmlin, C. Schubert, A. R. Kovsh, A. Jacob, A. Umbach, and D. Bimberg, "10 Gbit/s data modulation using 1.3 μ m InGaAs quantum dot lasers," Electron. Lett., vol. 41, no. 5, pp. 244-245, Mar. 2005.
- [19] K. Lüdge and E. Schöll, "Nonlinear dynamics of doped semiconductor quantum dot lasers," Eur. Phys. J. D, vol. 58, no. 2, pp. 167-174, Jun.
- [20] R. Wetzler, A. Wacker, and E. Schöll, "Self-consistent Coulomb effects and charge distribution of quantum dot arrays," Phys. Rev. B, vol. 68, no. 4, pp. 045323-1-045323-6, 2003.
- [21] T. R. Nielsen, P. Gartner, and F. Jahnke, "Many-body theory of carrier capture and relaxation in semiconductor quantum-dot lasers," Phys. Rev. B, vol. 69, no. 23, pp. 235314-1-235314-13, 2004.
- [22] D. Bimberg, M. Grundmann, and N. N. Ledentsov, Quantum Dot Heterostructures. New York: Wiley, 1999.
- [23] J. M. Pikal, C. S. Menoni, P. Thiagarajan, G. Y. Robinson, and H. Temkin, "Temperature dependence of intrinsic recombination coefficients in 1.3 µm InAsP/InP quantum-well semiconductor lasers," Appl. Phys. Lett., vol. 76, no. 19, pp. 2659-2661, May 2000.



Gerrit Fiol received the Diploma degree in physics from the Technische Universität Berlin, Berlin, Germany, in 2004. He is currently pursuing the Ph.D. degree at the Institute of Solid State Physics, Technische Universität Berlin.

His current research interests include quantum-dot photonic devices, especially mode-locked lasers.



Mirko Stubenrauch received the Diploma degree in physics from the Technische Universität Berlin, Berlin, Germany, in 2008.

He is currently with the Institut für Festkörperphysik, Technische Universität Berlin. His current research interests include modeling and fabrication of photonic quantum-dot devices, particularly highspeed QD lasers and modulators for optical data communication.



Dejan Arsenijević received the Diploma degree in physics from the Technische Universität Berlin, Berlin, Germany, in 2009. He is currently pursuing the Ph.D. degree in physics at the Technische Universität Berlin.

His current research interests include high-speed direct-modulated and mode-locked quantum-dot



Kathy Lüdge was born in Berlin, Germany, in 1976. She received the Diploma and the Dr. rer. nat. degrees in physics from the Department of Solid State Physics, Technische Universität Berlin, Berlin, in 2000 and 2003, respectively.

She was a Visiting Scholar with the Department of Material Science, University of Minnesota, Minneapolis, from 2001 to 2002. Currently, she is with the Institute of Theoretical Physics, Technische Universität Berlin. Her current research interests include modeling of semiconductor quantum-dot lasers, non-

linear laser dynamics, and control with optical feedback.



Roland Aust was born in Berlin, Germany, in 1980. He received the Diploma degree in physics from the Technische Universität Berlin, Berlin, in 2007. He is currently pursuing the Ph.D. degree at the Institute of Theoretical Physics, Technische Universität Berlin.

His current research interests include modeling of semiconductor quantum-dot lasers, nonlinear dynamics and control, noise, and delay differential equations.



Dieter Bimberg (F'10) received the Diploma degree in physics and the Ph.D. degree from Goethe University, Frankfurt, Germany, in 1968 and 1971, respectively.

He held the Principal Scientist position at the Max Planck-Institute for Solid State Research, Grenoble, France, and Stuttgart, Germany, from 1972 to 1979. In 1979, he was appointed a Professor of Electrical Engineering, Technical University of Aachen, Aachen, Germany. Since 1981, he has held the Chair of Applied Solid State Physics, Technische

Universität (TU) Berlin, Berlin, Germany. Since 1990, he has also been the Executive Director of the Solid State Physics Institute at TU Berlin. He was elected to the German Academy of Natural Sciences Leopoldina, Halle, Germany, in 2004. Since 2004, he has been the Director of the Center of Nanophotonics at TU Berlin. In 2006, he was elected Chairman of the Consortium of Nanotechnology Competence Centers in Germany (AGeNT-D). He has authored more than 900 papers, been awarded several patents, and written many books, resulting in more than 23 000 citations worldwide and an h-factor of 69. His current research interests include the physics of nanostructures and photonic devices, like quantum-dot lasers and amplifiers, single photon emitters, wide-gap semiconductor heterostructures, and ultrahigh-speed photonic devices.

Dr. Bimberg is a Fellow of the American Physical Society. He was the recipient of the Russian State Prize in Science and Technology in 2001, and the Max-Born Award and Medal in 2006.





Eckehard Schöll was born in Stuttgart, Germany, in 1951. He received the Diploma degree in physics from the University of Tübingen, Tübingen, Germany, in 1976, the Ph.D. degree in applied mathematics from the University of Southampton, Southampton, U.K., in 1978, and the Dr. rer. nat. degree and Venia Legendi from Aachen University of Technology, Aachen, Germany, in 1981 and 1986, respectively.

He was a Visiting Assistant Professor in the Department of Electrical and Computer Engineering, Wayne State University, Detroit, MI, from 1983 to 1984. Since 1989, he has been a Professor at the Institute of Theoretical Physics, Technische Universität Berlin, Berlin, Germany, and since 2001, has been its Director. He is the author of more than 350 research papers and three books, and the editor of several monographs and topical journal issues. His current research interests include nonlinear dynamics and control, pattern formation, chaos, noise, transport in semiconductor nanostructures, laser dynamics, and self-organized growth kinetics.

Dr. Schöll was the organizer of several international conferences including Dynamics Days Europe in 2005, and the 72nd Annual German Physical Society Meeting in 2008.